Targeted labeling of early-stage tumor spheroid in chorioallantoic membrane model with upconversion nanoparticles

Liu, K.; Holz, J.A.; Ding, Y.; Liu, X.; Zhang, Y.; Tu, L.; Kong, X.; Priem, B.; Nadort, A.; Lambrechts, S.A.G.; Aalders, M.C.G.; Buma, W.J.; Liu, Y.; Zhang, H.

DOI
10.1039/c4nr05638h

Publication date
2015

Document Version
Final published version

Published in
Nanoscale

Nanoscale

COMMUNICATION

View Article Online
View Journal | View Issue

Cite this: *Nanoscale*, 2015, **7**, 1596

Received 26th September 2014,
Accepted 26th October 2014

DOI: 10.1039/c4nr05638h

www.rsc.org/nanoscale

Targeted labeling of an early-stage tumor spheroid in a chorioallantoic membrane model with upconversion nanoparticles†

Kai Liu,‡[a,b,c] Jasmin A. Holz,‡[b] Yadan Ding,[b,c,d] Xiaomin Liu,[a] Youlin Zhang,[a] Langping Tu,[a] Xianggui Kong,*[a] Bram Priem,[b] Annemarie Nadort,[b] Saskia A. G. Lambrechts,[b] Maurice C. G. Aalders,*[b] Wybren Jan Buma,[c] Yichun Liu[d] and Hong Zhang*[c]

***In vivo* detection of cancer at an early-stage, *i.e.* smaller than 2 mm, is a challenge in biomedicine. In this work target labeling of an early-stage tumor spheroid (~500 μm) is realized for the first time in a chick embryo chorioallantoic membrane (CAM) model with monoclonal antibody functionalized upconversion nanoparticles (UCNPs-mAb).**

In clinical oncology the detection of early-stage cancer like carcinoma *in situ* and tumors smaller than 2 mm is of great importance for improving the cancer cure probability.[1–3] Unfortunately, most of the present clinical imaging modalities like ultrasonic imaging, computed tomography (CT), and magnetic resonance imaging (MRI) are not sufficient for detecting the early-stage cancers because of their low resolution and/or poor sensitivity and/or specificity.[4,5] Fluorescence imaging has recently regained increased attention for cancer diagnosis, because of the new developments in exogenous luminescent materials,[6–14] such as rare earth ion doped upconversion nanoparticles (UCNPs) that can efficiently convert near infrared (NIR) light to visible and/or shorter wavelength NIR light. In comparison with traditional "down conversion" fluorescent markers that need ultra-violet or visible (UV-Vis) light for excitation, the UCNPs hold many advantages for biomedical imaging, such as minimized background fluorescence, and no photo bleaching.[11–14] Furthermore, since UCNPs have a large surface area, bio-functionalized molecules like folic acid, peptides, photosensitizers, doxorubicin (DOX), and si-RNA can be easily conjugated for multifunctional labeling or therapy. Numerous research studies have been reported in this respect on both *in vitro* and *in vivo* tests utilizing UCNPs.[15–25] For example, Zhou *et al.* achieved tri-mode imaging of upconversion luminescence, magnetic resonance and positron emission tomography (PET) in mouse utilizing fluorine-18-labeled Gd^{3+}/Yb^{3+}/Er^{3+} co-doped $NaYF_4$ UCNPs.[23] However, these research studies are performed on the mice model in which the imaging is usually executed at a relatively late stage when tumors reach 4–6 mm. *In vivo* target detection of early stage cancer, *i.e.* smaller than 2 mm, remains a difficult task in biomedicine.

In this work, target labeling of an early-stage tumor spheroid (~500 μm) was realized for the first time in a chick embryo chorioallantoic membrane (CAM) model with monoclonal antibody functionalized upconversion nanoparticles (UCNPs-mAb). An early-stage tumor spheroid model was built first by transplanting an *in vitro* cultured 3 dimensional multicellular tumor spheroid (MCTS) of human breast cancer cells MCF-7 onto the chick embryo CAM. The chick embryo CAM is a well-established model which has already been widely used for cancer and angiogenesis research, drug delivery, immunology *etc.*[26–34] Compared with the widely used mice model, the chick embryo CAM has unique advantages in cancer research, including (i) the chick embryo is a naturally immunodeficient system, and various heterogeneous tumor cells can be transplanted into the CAM without any species-specific restrictions, and (ii) since the chick embryo CAM is an extremely thin membrane layer (~200 μm) that usually lies at the top, it is very convenient to observe the motility process of the injected cancer cells or drug molecules under a microscope with little impact on the host. On top of that, the chick embryo model is simple

[a]*State Key Laboratory of Luminescence and Application, Changchun Institute of Optics, Fine Mechanics and Physics, Chinese Academy of Science, Changchun 130033, P. R. China. E-mail: xgkong14@ciomp.ac.cn*
[b]*Department of Biomedical Engineering and Physics, Academic Medical Center, University of Amsterdam, 1105 AZ Amsterdam, P.O. Box 22700, The Netherlands. E-mail: m.c.aalders@amc.uva.nl*
[c]*Van't Hoff Institute for Molecular Sciences, University of Amsterdam, Science Park 904, 1098 XH Amsterdam, The Netherlands. E-mail: h.zhang@uva.nl*
[d]*Centre for Advanced Optoelectronic Functional Materials Research, Key Laboratory for UV Light-Emitting Materials and Technology of the Ministry of Education, Northeast Normal University, Changchun 130024, P. R. China*
†Electronic supplementary information (ESI) available: Details of experimental procedures for the sample preparation and characterization, Chick CAM model, 3-D multicellular tumor spheroids, UCNPs circulating in CAM. See DOI: 10.1039/c4nr05638h
‡These authors contributed equally to this article.

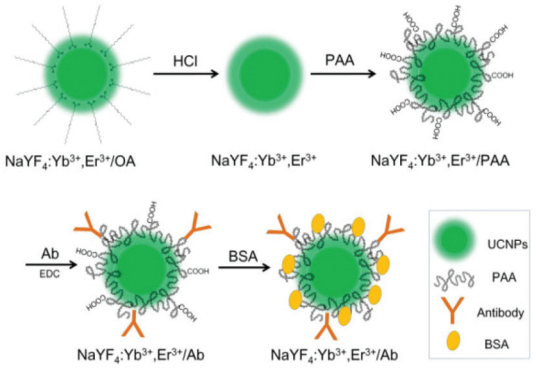

Fig. 1 Construction of a UCNPs-mAb nanoplatform.

(without animal manipulation), low cost, easy to maintain, and easily accessible. Since the MCF-7 cell line has a high expression level of estrogen receptor alpha (ER-α), the corresponding monoclonal antibodies (mAb) of ER-α were covalently functionalized onto the polyacrylic acid (PAA) stabilized $NaYF_4$:Yb^{3+},Er^{3+} UCNPs *via* a simple EDC cross-linking method (as illustrated in Fig. 1), aiming to achieve a highly sensitive upconversion luminescence (UCL) imaging nanoplatform for target labeling of the early stage tumor spheroid transplanted in the chick embryo CAM.

The surface modification process was carried out to transfer the hydrophobic $NaYF_4$:Yb^{3+},Er^{3+} UCNPs synthesized from an organic solvent into hydrophilic ones *via* a simple two-step ligand exchange method. As illustrated in Fig. 1, the oleic acid (OA) capped outside UCNPs were removed by protonation treatment to obtain ligand free UCNPs,[35,36] followed by the treatment with poly acrylic acid on the ligand free nanoparticles, anchoring the UCNPs with carboxylic groups. Fig. 2A and B show the TEM images of ligand free and PAA coated $NaYF_4$:Yb^{3+},Er^{3+} UCNPs. Both ligand free and PAA coated nanoparticles have good dispersibility and uniform size distribution with an average size of around 45 nm. Fig. 2C shows the high resolution TEM image of an individual nanoparticle, where the lattice fringes with interplanar spacing are about 0.52 nm, corresponding to the (100) plane of hexagonal-phase structured $NaYF_4$. The inset shows the fast Fourier-transform (FFT) diffractogram, confirming the hexagonal-phase of the UCNPs. To prove that the PAA molecules were capped on $NaYF_4$:Yb^{3+}, Er^{3+} UCNPs, Fourier transform infrared spectroscopy (FTIR) characterization was performed (Fig. 2D).

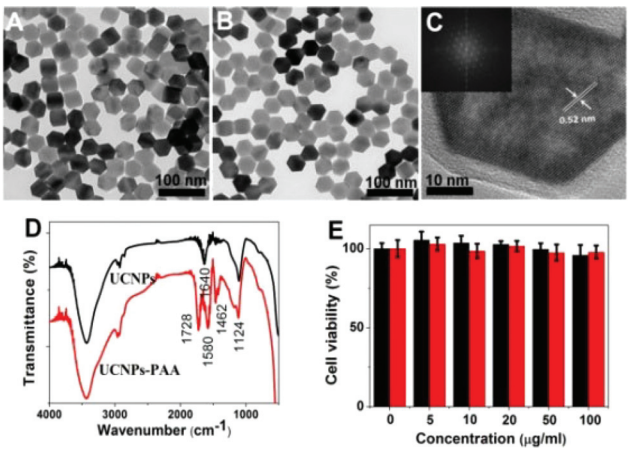

Fig. 2 (A) TEM image of ligand free $NaYF_4$:Yb^{3+},Er^{3+} UCNPs. (B) PAA coated UCNPs. (C) TEM image of a single nanoparticle, with the corresponding diffractogram (insert). (D) FTIR spectra of ligand free UCNPs and PAA coated UCNPs. (E) Cellular viability results based on the standard MTT assay.

The band around 1124 cm^{-1} is due to the C–O stretching vibration of the carboxyl groups, and the two strong bands centered at 1580 cm^{-1} and 1462 cm^{-1} are associated with the asymmetric and symmetric stretching vibration modes of the carboxylate anions, suggesting the effective COO-RE^{3+} complexation on the UCNP surface. The band at 1728 cm^{-1} is assigned to the C=O stretching vibration of the free carboxyl groups on the PAA polymer chain.

It is known that the hydrodynamic diameters and surface charges affect greatly cellular endocytosis and toxicity.[37–41] Therefore, we have measured the hydrodynamic diameters and zeta-potential and the results are shown in Fig. S1.† Compared with the ligand free nanoparticles, an increase in hydrodynamic diameters was observed in PAA coated nanoparticles, which may indicate the dwelling effect of polymer layers coated on the surface of UCNPs. A significant change was also observed in the surface charges, varying from 45.5 mV (ligand free UCNPs) to −37.9 mV (PAA coated UCNPs), confirming the existence of carboxyl groups at the surface of UCNPs. The UCL spectra of the ligand free and PAA coated $NaYF_4$:Yb^{3+}, Er^{3+} UCNPs with the same concentration (1 mg mL^{-1}) in water at 980 nm excitation of 400 mW are given in Fig. S2.† The upconversion luminescence in the visible region has two bands, a green one around 515–560 nm and a red one around 640–675 nm, which are ascribed to transitions of $^4S_{3/2}$–$^4I_{15/2}$ and $^4F_{9/2}$–$^4I_{15/2}$ from the doped Er^{3+} ions, respectively. The two UCL spectra are similar, indicating that the polymer coating has a negligible effect on the luminescence properties of the UCNPs.

Cytotoxicity was investigated on two different cell lines, human breast adenocarcinoma MCF-7 and mouse embryo fibroblast 3T3, using different concentrations of UCNPs-mAb conjugates (0, 5, 10, 20, 50, and 100 μg mL^{-1}). After 24 h, no significant change was observed in the cell morphology and proliferation of both cell lines in the presence of the UCNPs-mAb conjugates. The cellular viability was evaluated by the MTT assay of the mitochondrial activities and relevant results are shown in Fig. 2E. Both cell lines demonstrate good viability, even at the maximum concentration of 100 μg mL^{-1}, and the viability is greater than 90%. These results indicate that UCNPs-mAb conjugates have good biocompatibility and could be used for *in vivo* imaging. Fig. 3 shows the confocal microscopy images of MCF-7 breast adenocarcinoma cells (positive) and 3T3 fibroblast cells (negative) after treatment with UCNPs-mAb (100 μg mL^{-1}) for 8 h. The bright field images show that the cellular morphology is intact, which is

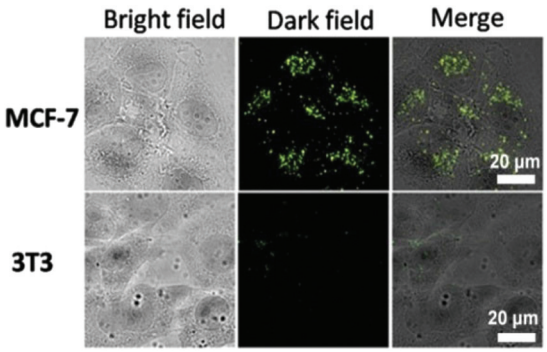

Fig. 3 Confocal upconversion luminescence images at 100× magnification of UCNPs-mAb incubated with MCF-7 cells (top row) and 3T3 cells (bottom row) for 8 h at 37 °C.

consistent with the cytotoxicity results of the UCNPs-mAb conjugates. The dark field images show the upconversion luminescence within the MCF-7 cells, whereas little luminescence was observed in the 3T3 cells. The latter is related to the residual non-specific adsorption of the UCNPs on the 3T3 cell membranes. These results indicate that the UCNPs-mAb conjugates can specifically label on the MCF-7 breast cancer cells.

In our study a shell-less cultured chick embryo was developed as the model to research the *in vivo* labeling properties of UCNPs-mAb. A typical shell-less chick embryo is shown in Fig. S3.† The CAM membrane is settled on the top of embryo and yolk, and the blood vessels of CAM can be seen very clearly with naked eyes. In order to assess the *in vivo* targeting behavior of the UCNPs-mAb conjugates on early stage cancer spheroids, MCTSs were cultured *in vitro* and transplanted onto the CAM. Compared with the cancer cells cultured in 2-D, the MCTS show a condensed structure in 3-D (Fig. S4†), and can mimic more closely the cellular–matrix and cell–cell interactions *in vivo*.[42] After 3 days of incubation, the MCTS could be embedded into the CAM membrane (Fig. S5†), and the newly grown blood vessels can be clearly seen surrounding the MCTS. Then UCNPs-mAb were systematically administrated into the chick embryo CAM *via* venule injection under a stereomicroscope. Owing to the depression of autofluorescence during UCL imaging, the microcirculating behavior of the nanoconjugates in blood vessels was able to be neatly investigated with a modified fluorescence intravital microscope that was equipped with a 980 nm laser. As shown in Fig. S6,† on the left is the white image of a typical CAM blood vessel net, and on the right is the corresponding upconversion luminescence image 10 min after the injection of UCNPs-mAb conjugates. We can distinctly see that the nanoparticles fluently flow with the bloodstream and efficiently extravasate from the main blood vessels into the surrounding tissues. Thus the CAM model provides us a simple approach for real-time visualizing the *in situ* interaction of nanoparticles with the vascular networks and also the biotissues, which might be of great value for future nano-bio research studies.

The *in situ* upconversion luminescence imaging of the tumor spheroid was then investigated at different times with

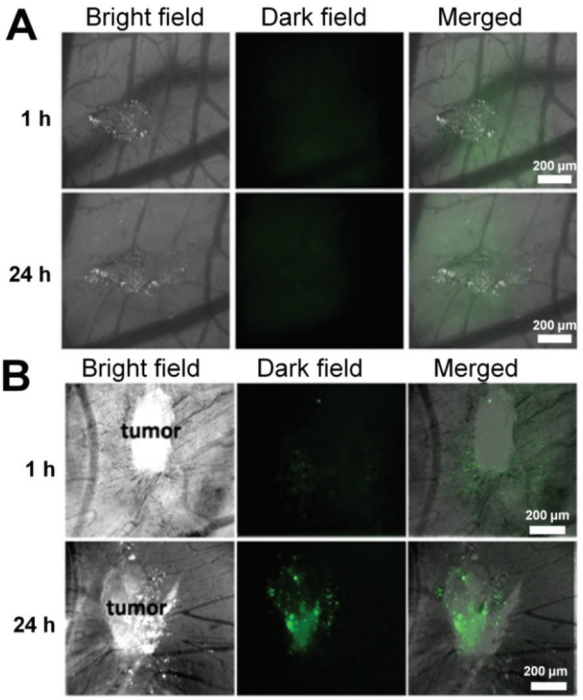

Fig. 4 Non-targeted (A) and targeted (B) labeling of MCTS transplanted on the CAM with UCNPs at 1 h (top row) and 24 h (bottom row). From left to right are bright field, dark field (980 nm irradiation) and merged intravital microscopy images at 4× magnification and 2 min exposure time.

an intravital microscope. The UCNPs without any antibody functionalization (non-functionalized UCNPs) were also injected for control, data are shown in Fig. 4A. We see that the non-functionalized UCNPs were present in both the MCTS and the surrounding tissue without specific accumulation within the MCTS, both at 1 h and at 24 h after injection. In contrast, the functionalized UCNPs-mAb were accumulated specifically on the MCTS (Fig. 4B). One hour after injection, the UCNPs-mAb were observed mainly in the surrounding tissue of the MCTS. Twenty-four hours after injection, strong upconversion luminescence was obviously observed in the MCTS, indicating the good targeted delivery of UCNPs-mAb conjugates.

In order to further demonstrate the selective labeling of UCNPs-mAb in tumor cells, the resected MCTS region was histologically examined (Fig. 5). Fig. 5A shows the microscopy image of the H&E stained MCTS embedded into the CAM tissue. Fig. 5B and C are the confocal upconversion luminescence images of CAM and MCTS corresponding to the marked areas in Fig. 5A. As expected, normal CAM regions show very low amount or no luminescence of UCNPs-mAb (Fig. 5B), whereas targeted luminescence of UCNPs-mAb was only observed in the transition zone from the CAM into the MCTS (Fig. 5C). Low fluorescence was detected from the surrounding tissue, resulting in a high contrast between targeted MCF-7 cells and the surrounding tissue. In contrast, from the histological examination of MCTS administered with non-functionalized UCNPs, only very little amount of upconversion luminescence was observed in the MCTS.

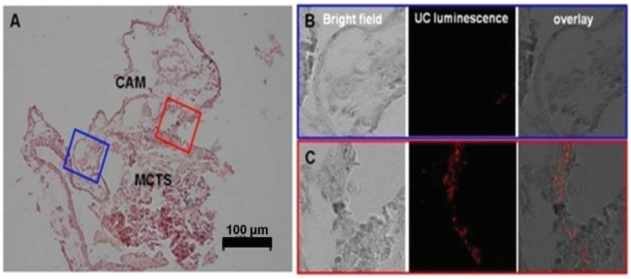

Fig. 5 H&E-stained section (A) of MCTS on the CAM, 30 min after UCNP-mAb injection. (B) Shows the upconversion luminescence of the surrounding CAM. (C) Shows the upconversion luminescence of the transition zone between CAM and MCTS. Scale bar is 100 μm.

Conclusions

In conclusion, $NaYF_4$:Yb,Er upconversion nanoparticles have been successfully functionalized and employed for target labeling the cancer at an early stage in the CAM model. PAA coated UCNPs were synthesized by a two-step ligand exchange method, and functionalized with ER-α monoclonal antibodies to obtain UCNPs-mAb conjugates. *In vitro* research studies reveal that the UCNPs-mAb conjugates have no significant cytotoxicity on mammalian cells, and can specifically label in the MCF-7 breast cancer cells rather than in the normal cells. The cellular viability was higher than 90% even at a relatively high concentration (100 μg mL^{-1}) of UCNPs-mAb. The 3-dimensional MCTS (~500 μm) transplanted CAM model has been developed as the early stage tumor model to research the *in vivo* labeling properties of UCNPs-mAb. Intravital microscopy imaging demonstrated that intravenously injected UCNPs-mAb conjugates have high specificity in labeling the breast cancer. Our work suggests that UCNPs-mAb, in combination with CAM, offer a new possibility in early cancer studies.

This work was supported by the NSF of China (11174277, 11374297, 61275202, 21304084, 1174278), a joint research program between CAS of China and KNAW of the Netherlands, the IOP program of the Netherlands and John van Geuns funds.

Notes and references

1 R. A. Smith, V. Cokkinides, A. C. von Eschenbach, B. Levin, C. Cohen, C. D. Runowicz, S. Sener, D. Saslow, H. J. Eyre and American Cancer Society, *CA Cancer J. Clin.*, 2002, **52**, 8–22.
2 S. R. Hingorani, E. F. Petricoin, A. Maitra, V. Rajapakse, C. King, M. A. Jacobetz, S. Ross, T. P. Conrads, T. D. Veenstra, B. A. Hitt, *et al.*, *Cancer Cell*, 2003, **4**, 437–450.
3 M. S. Rahman, N. Ingole, D. Roblyer, V. Stepanek, K. R. Richards, A. Gillenwater, S. Shastri and P. Chaturvedi, *Head Neck Oncol.*, 2010, **2**, 10.
4 D. A. Benaron, *Cancer Metast. Rev.*, 2002, **21**, 45–78.
5 R. Weissleder, *Nat. Rev. Cancer*, 2002, **2**, 1–8.
6 U. Mahmood, C. H. Tung, A. Bogdanov and R. Weissleder, *Radiology*, 1999, **213**, 866–870.
7 X. He, K. Wang and Z. Cheng, *Wiley Interdiscip. Rev. Nanomed. Nanobiotechnol.*, 2010, **2**, 349–366.
8 X. Michalet, F. F. Pinaud, L. A. Bentolila, J. M. Tsay, S. Doose, J. J. Li, G. Sundaresan, A. M. Wu, S. S. Gambhir and S. Weiss, *Science*, 2005, **307**, 538–544.
9 W. Cai, D. W. Shin, K. Chen, O. Gheysens, Q. Cao, S. X. Wang, S. S. Gambhir and X. Chen, *Nano Lett.*, 2006, **6**, 669–676.
10 G. Chen, H. Qiu, P. N. Prasad and X. Chen, *Chem. Rev.*, 2014, **114**, 5161–5214.
11 Y. Park, J. H. Kim, K. T. Lee, K. S. Jeon, H. B. Na, J. H. Yu, H. M. Kim, N. Lee, S. H. Choi, S. Baik, *et al.*, *Adv. Mater.*, 2009, **21**, 4467–4471.
12 D. K. Chatterjee, A. J. Rufaihah and Y. Zhang, *Biomaterials*, 2008, **29**, 937–943.
13 L. C. Ong, L. Y. Ang, S. Alonso and Y. Zhang, *Biomaterials*, 2014, **35**, 2987–2998.
14 L. L. Li, P. Wu, K. Hwang and Y. Lu, *J. Am. Chem. Soc.*, 2013, **135**, 2411–2414.
15 M. Wang, C. C. Mi, W. X. Wang, C. H. Liu, Y. F. Wu, Z. R. Xu, C. B. Mao and S. K. Xu, *ACS Nano*, 2009, **3**, 1580–1586.
16 L. Xiong, Z. Chen, Q. Tian, T. Cao, C. Xu and F. Li, *Anal. Chem.*, 2009, **21**, 8687–8694.
17 M. K. Jayakumar, A. Bansal, K. Huang, R. Yao, B. N. Li and Y. Zhang, *ACS Nano*, 2014, **8**, 4848–4858.
18 Y. Sun, X. Zhu, J. Peng and F. Li, *ACS Nano*, 2013, **7**, 11290–11300.
19 D. Ni, J. Zhang, W. Bu, H. Xing, F. Han, Q. Xiao, Z. Yao, F. Chen, Q. He, J. Liu, *et al.*, *ACS Nano*, 2014, **8**, 1231–1242.
20 K. Liu, X. Liu, Q. Zeng, Y. Zhang, L. Tu, T. Liu, X. Kong, Y. Wang, F. Cao, S. A. Lambrechts, *et al.*, *ACS Nano*, 2012, **6**, 4054–4062.
21 F. Wang and X. Liu, *J. Am. Chem. Soc.*, 2008, **130**, 5642–5643.
22 L. Xia, X. Kong, X. Liu, L. Tu, Y. Zhang, Y. Chang, K. Liu, D. Shen, H. Zhao and H. Zhang, *Biomaterials*, 2014, **35**, 4146–4156.
23 J. Zhou, M. Yu, Y. Sun, X. Zhang, X. Zhu, Z. Wu, D. Wu and F. Li, *Biomaterials*, 2011, **32**, 1148–1156.
24 H. Xing, W. Bu, S. Zhang, X. Zheng, M. Li, F. Chen, Q. He, L. Zhou, W. Peng, Y. Hua and J. Shi, *Biomaterials*, 2012, **33**, 1079–1089.
25 X. Wang, K. Liu, G. Yang, L. Cheng, L. He, Y. Liu, Y. Li, L. Guo and Z. Liu, *Nanoscale*, 2014, **6**, 9198–9205.
26 J. D. Lewis, G. Destito, A. Zijlstra, M. J. Gonzalez, J. P. Quigley, M. Manchester and H. Stuhlmann, *Nat. Med.*, 2006, **12**, 354–360.
27 A. Vargas, M. Zeisser-Labouèbe, N. Lange, R. Gurny and F. Delie, *Adv. Drug Delivery Rev.*, 2007, **59**, 1162–1176.
28 H. S. Leong, N. F. Steinmetz, A. Ablack, G. Destito, A. Zijlstra, H. Stuhlmann, M. Manchester and J. D. Lewis, *Nat. Protoc.*, 2010, **5**, 1406–1417.
29 N. A. Lokman, A. S. Elder, C. Ricciardelli and M. K. Oehler, *Int. J. Mol. Sci.*, 2012, **13**, 9959–9970.

30 J. Borges, F. T. Tegtmeier, N. T. Padron, M. C. Mueller, E. M. Lang and G. B. Stark, *Tissue Eng.*, 2003, **9**, 441–450.
31 D. Ribatti, B. Nico, A. Vacca, L. Roncali, P. H. Burri and V. Djonov, *Anat. Rec.*, 2001, **264**, 317–324.
32 W. W. Chin, W. K. Lau, R. Bhuvaneswari, P. W. Heng and M. Olivo, *Cancer Lett.*, 2007, **245**, 127–133.
33 C. Cho, A. Ablack, H. Leong, A. Zijlstra and J. Lewis, *J. Vis. Exp.*, 2011, **52**, e2808, DOI: 10.3791/2808.
34 I. E. Deryugina and J. P. Quigley, *Histochem. Cell Biol.*, 2008, **130**, 1119–1130.
35 N. Bogdan, F. Vetrone, G. A. Ozin and J. A. Capobianco, *Nano Lett.*, 2011, **11**, 835–840.
36 N. Bogdan, E. M. Rodríguez, F. Sanz-Rodríguez, M. C. Cruz, Á. Juarranz, D. Jaque, J. G. Solé and J. A. Capobianco, *Nanoscale*, 2012, **4**, 3647–3650.
37 J. Jin, Y. J. Gu, C. W. Y. Man, J. Cheng, Z. Xu, Y. Zhang, H. Wang, V. H. Y. Lee, S. H. Cheng and W. T. Wong, *ACS Nano*, 2011, **5**, 7838–7847.
38 A. M. Alkilany and C. J. Murphy, *J. Nanopart. Res.*, 2010, **12**, 2313–2333.
39 A. M. El Badawy, R. G. Silva, B. Morris, K. G. Scheckel, M. T. Suidan and T. M. Tolaymat, *Environ. Sci. Technol.*, 2010, **45**, 283–287.
40 J. Jiang, G. Oberdorster and P. Biswas, *J. Nanopart. Res.*, 2009, **11**, 77–89.
41 A. Albanese, P. S. Tang and W. C. Chan, *Annu. Rev. Biomed. Eng.*, 2012, **14**, 1–16.
42 H. L. Ma, Q. Jiang, S. Han, Y. Wu, T. J. Cui, D. Wang, Y. Gan, G. Zou and X. J. Liang, *Mol. Imaging*, 2012, **11**, 487–498.

